AIAA JOURNAL
Vol. 36, No. 4, April 1998

Feasibility Study of Magnetohydrodynamics Acceleration of Unseeded and Seeded Airflows

Igor V. Adamovich* and J. William Rich†
Ohio State University, Columbus, Ohio 43210-1107
and
Gordon L. Nelson‡
MSE Inc., Butte, Montana 59702

Nonequilibrium, reacting, ionized gas flow modeling is used to study the feasibility of magnetohydrodynamics (MHD) acceleration of airflows for the energy addition wind tunnel. The kinetic model incorporates equations of one-dimensional magnetogasdynamics, the master equation for vibrational level populations of diatomic species, equations of chemical and ionization kinetics, and the Boltzmann equation for electrons. The model is validated by comparison with the experiments in MHD accelerators. Calculations are made for two accelerator schemes, the first using an electron beam to sustain nonequilibrium ionization in unseeded air and the second using alkali-seeded air. The results are compared with the target flow parameters of the transatmospheric vehicle. The unseeded flow calculations show that the use of external ionization in high-pressure MHD flows is inefficient due to fast electron loss. Although at low pressures external ionization allows substantial increase of the flow total enthalpy, the obtained test section pressure is much lower than required, and the flow quality is poor. Calculations for alkali-seeded flows predict test section flow parameters closer to the target values, with O atom and NO concentrations lower than in the e-beam-controlled flows. Flow stability is analyzed using the linear stability theory. A thermodynamic energy addition criterion is used to demonstrate the advantage of direct kinetic energy increase in MHD acceleration over thermal energy addition methods.

Nomenclature

$\boldsymbol{B}$	= magnetic field, T
D	= electron beam load, eV/mol/s
$\boldsymbol{E}$	= electric field, V/m
E/N	= reduced electric field, 10^{-17} V · cm^2
F	= cross-sectional area, m^2
$f(\varepsilon)$	= electron energy distribution
G	= mass flow rate, kg/s
H	= total enthalpy, J/kg
h	= magnetohydrodynamics (MHD) channel half-width, m
I	= ionization potential, K
$\boldsymbol{j}$	= current density, A/m^2
K	= loading parameter
L	= MHD channel length, m
l	= e-beam penetration length, m
M	= Mach number
N	= number density, m^{-3}
n_e	= electron concentration, m^{-3}
$n(v)$	= vibrational level populations, m^{-3}
P	= static pressure, atm
P_{dyn}	= dynamic pressure, lb/ft^2
Q	= power added to the flow, J/kg
Re	= Reynolds number
S	= entropy, J/kg/K
T	= temperature, K
T_e	= electron temperature, K
T_v	= vibrational temperature, K
u	= flow velocity, m/s
v	= vibrational quantum number
x	= axial coordinate, m
y, z	= transverse coordinates, m
β	= Hall parameter
γ	= specific heat ratio
δ	= boundary-layer thickness, m
ε	= electron energy, eV
θ	= first vibrational level energy, K
ρ	= flow density, kg/m^3
σ	= electric conductivity, Ω^{-1} m^{-1}
Ω	= instability increment

Subscripts

avg	= average
beam	= electron beam
eff	= effective
flight	= freestream
i	= ith species
max	= maximum
0	= plenum
1	= MHD channel entrance
2	= MHD channel exit

I. Introduction

THE present paper addresses the feasibility of magnetohydrodynamics (MHD) acceleration of high-pressure supersonic airflows. The main objective is to explore the applicability of MHD augmentation for use in the next-generation energy addition wind tunnels. These facilities are under development for studies of high-speed combustion and testing hypersonic air-breathing engines.[1–3] The basic design requirements that determine the performance objectives of MHD accelerators for such facilities are as follows.[3–6]

1) The flow parameters, such as Mach number, total enthalpy, entropy, and chemical composition, should simulate the conditions behind the bow shock of the hypersonic aircraft corresponding to the 2000-lb/ft^2 freestream dynamic pressure trajectory. In particular, the flow should have minimum dissociation and contamination.

2) The test area cross section should be about 8 m^2 to enable full-scale engine testing.

3) A test duration on the order of tens of seconds to minutes should be available.

The first of these requirements encourages exploring the possibility of efficient MHD acceleration of airflows without using easily

Presented as Paper 96-2347 at the AIAA 27th Plasmadynamics and Lasers Conference, New Orleans, LA, June 17–20, 1996; received Aug. 8, 1997; revision received Dec. 15, 1997; accepted for publication Dec. 18, 1997.

*Research Scientist, Department of Mechanical Engineering. Senior Member AIAA.

†Ralph W. Kurtz Professor, Department of Mechanical Engineering. Associate Fellow AIAA.

‡Staff Engineer in Aerospace Programs. Senior Member AIAA.

ionized seeds, e.g., alkali atoms, but relying on external ionization sources, such as electron beams, instead.

The major technical issues addressed in the paper include 1) the use of a high-energy electron beam to enhance the unseeded airflow conductivity in the MHD channel, 2) the analysis of seeded vs unseeded flow accelerator performance, and 3) the fundamental thermodynamic limits of MHD drivers. The analysis is based on a one-dimensional nonequilibrium ionized flow modeling. Similar studies have been conducted previously.[4–6] However, the present approach incorporates several novel features, such as 1) the incorporation of an advanced model for nonequilibrium ionized air chemistry, 2) the incorporation of the Boltzmann equation for electrons, 3) the ability to simulate the flow ionization by an electron beam directed into the MHD channel, and 4) the ability to model coupled nonequilibrium vibrational kinetics, chemical kinetics, and kinetics of electrons. Details of the kinetic model are given in Sec. II. Modeling calculations were made across a wide range of parameters, such as electron beam energy, seed fraction and type, plenum pressures and temperatures, and nozzle geometry (see Sec. III). The conclusions are given in Sec. IV.

II. Kinetic Modeling

A. Kinetic Equations

To simulate the gasdynamics and kinetics of both alkali-seeded and unseeded airflows in supersonic nozzles and MHD channels, we have used quasi-one-dimensional nonequilibrium flow modeling. The model incorporates the following equation groups: 1) the equations of magnetogasdynamics for nonequilibrium reacting real gases[7,8]; 2) the chemical and ionization kinetics equations for reacting species, including electrons, ions, and excited metastable species[9] (nonequilibrium vibrationally induced chemical reactions, e.g., dissociation and bimolecular exchange reactions, and field-induced processes, e.g., electron impact excitation and ionization, are taken into account); 3) the master equation for vibrational level populations $n_i(v)$ of diatomic species N_2, O_2, and NO (Refs. 9 and 10) {the population change due to vibration-translation (V-T), vibration-vibration (V-V), and electron-vibration (e-V) energy transfer processes and chemical reactions is taken into account; the vibrational temperatures of the species are given as $T_{v,i} = \theta_i / \ln[n_i(1)/n_i(0)]$}; 4) the Boltzmann equation for the electron energy distribution function $f(\varepsilon)$ in crossed fields[11,12] (it takes into account momentum transfer collisions; rotational, vibrational, and electronic excitation; electron-electron collisions; ionization; and attachment; superelastic processes that heat the electrons in vibrationally nonequilibrium gas flows[13,14] are also incorporated; the electron temperature is defined as $T_e = \{f(\varepsilon) \cdot [\mathrm{d}f(\varepsilon)/\mathrm{d}\varepsilon]^{-1}\}_{\varepsilon=0}$); and 5) the generalized Ohm's law[8] [in this one-dimensional approach, the electric and magnetic fields are given as functions of the axial coordinate x: $E_x(x)$, $E_y(x)$, and $B_z(x)$].

The effects of vibrational relaxation and chemical reactions are accounted for in the energy and motion equations, group 1. The chemistry-vibration coupling terms are incorporated into the chemical kinetics equations, group 2, and the master equation, group 3. Electron impact process rates used in kinetic equations, groups 2 and 3, as well as electric conductivity used in Ohm's law, group 5, are obtained from the Boltzmann equation, group 4, which couples vibrational and electron mode energies. Therefore, the system of equations solved is self-consistent.

B. Rates and Cross Sections

The neutral species chemical reaction rates at thermal equilibrium (32 reactions for 12 species, N, N_2, O, O_2, NO, O_3, NO_2, N_2O, NO_3, N_2O_4, N_2O_5, and N_3) are taken from Ref. 15. The vibration-chemistry coupling is simulated using the Macheret–Fridman–Rich nonequilibrium model,[16,17] and the state-specific rates for the reactions

$$\begin{aligned} N_2(v) + M &\leftrightarrows N + N + M \\ O_2(v) + M &\leftrightarrows O + O + M \\ NO(v) + M &\leftrightarrows N + O + M \\ N_2(v) + O &\leftrightarrows NO + N \\ NO(v) + O &\leftrightarrows O_2 + N \end{aligned} \qquad (1)$$

used in chemical and vibrational kinetics equations are the same as in Ref. 18.

The ion-molecular reactions rates (more than 300 reactions for 13 species, e^-, N^+, N_2^+, O^+, O_2^+, NO^+, O^-, O_2^-, N_2O^+, NO_2^-, Na^+, K^+, and Cs^+) were taken from Refs. 19–23. The rates of electron impact ionization and electron attachment for N_2, O_2, NO, Na, K, and Cs are calculated by the Boltzmann equation solver using the experimental cross sections.[24–27] The latter group of processes describes kinetics of nonequilibrium ionization and attachment of the plasma electrons in the presence of external electric and magnetic fields.

Thermochemical data for all species in the temperature range 300–6000 K (Refs. 28 and 29) are incorporated into the code. Therefore the kinetic model correctly predicts the chemical composition of ionized alkali-seeded air in equilibrium (with no fields applied).

The rates of electronic excitation and dissociation of N_2 and O_2 by the plasma electrons, with the production of metastable species $N_2(A^3\Sigma_u^+)$, $N(^2D)$, $N(^2P)$, $O_2(a^1\Delta_g)$, $O_2(b^1\Sigma_g^+)$, $O(^1D)$, and $O(^1S)$, are calculated by the Boltzmann solver using the experimental cross sections.[24,25] Metastable species chemical reaction rates are taken from Ref. 19.

The rates of vibrational excitation of N_2 and O_2 by plasma electrons are evaluated by the Boltzmann solver using the cross sections[24,25] and the semiempirical method,[30] e.g., see Ref. 12. The V-T and V-V rates for N_2 and O_2 are the same as in Ref. 18, where they are calculated by the forced harmonic oscillator rate model.[31] The V-T rates for N_2-Na, N_2-K, and N_2-Cs are taken from Refs. 32 and 33.

The electron transport cross sections for N_2, O_2, NO, Na, K, and Cs for the electric conductivity calculations are taken from Refs. 24–26 and 34.

In the present calculations, we considered the use of an electron beam as the most efficient way to sustain nonequilibrium ionization. It is well known that up to 50% of the relativistic e-beam power goes into electron impact ionization.[19] This ionization method has been used extensively to sustain a discharge in supersonic flows in gasdynamic lasers.[35] The e-beam power fractions going into ionization, dissociation, and electronic excitation of N_2 and O_2 in air are taken from Ref. 19. In the present study we do not address the engineering issues, such as a beam entering the high-pressure flow, focusing, x-ray radiation, etc. Our primary interest is the e-beam-initiated kinetics.

Wall heat transfer and skin-friction coefficients are calculated using the results of turbulent compressible boundary-layer theory.[36] Heat fluxes to the electrode surfaces are calculated based on the experimental heat transfer measurements in MHD accelerators.[37]

C. Code Validation

Parts of the kinetic model used in the present paper have been previously validated in modeling calculations. First, V-T and V-V rates, chemical reaction rates, and vibration-chemistry coupling in high-temperature air were validated by modeling of NO radiation behind shock waves, which showed good agreement with time-resolved shock tube measurements.[18] Second, electron swarm parameters in air, predicted by the Boltzmann equation solver, are in very good agreement with available experimental data.[11,38]

We have also made two series of validation calculations for the entire model. The results of the first series were compared with the data (somewhat scarce) obtained on the General Electric (GE) unseeded air MHD accelerator.[39,40] In these experiments, air was heated up to $T_0 = 9500$ K at a pressure $P_0 = 550$ atm behind the reflected shock and then expanded through a MHD channel ($L =$ 30 cm, $F_1 = 1\ \mathrm{cm}^2$, $F_2/F_1 = 2.0$, $B = 4.2$ T, and test time $\sim$1 ms). The test section impact pressure measured in the MHD-augmented flow was 1.5–2 times higher than in the isentropic flow. Figure 1 shows calculated axial profiles of the gas temperature and velocity for both MHD-augmented and isentropic flow, as well as the velocity profile obtained from the GE group one-dimensional equilibrium flow model.[39] The good agreement between these two models, both predicting about 15% velocity increase, is due to the fact that, at the high temperature $T \cong 6800$ K and pressure $P = 10$–30 atm, the flow in the channel is close to equilibrium. The effective reduced electric field was also low:

$$\left(\frac{E}{N}\right)_{\mathrm{eff}} = \frac{1}{N}\left[\frac{E_x^2 + (E_y - uB_z)^2}{1+\beta^2}\right]^{\frac{1}{2}} \leq 10^{-17}\ \mathrm{V \cdot cm^2} = 1\ \mathrm{Td} \qquad (2)$$

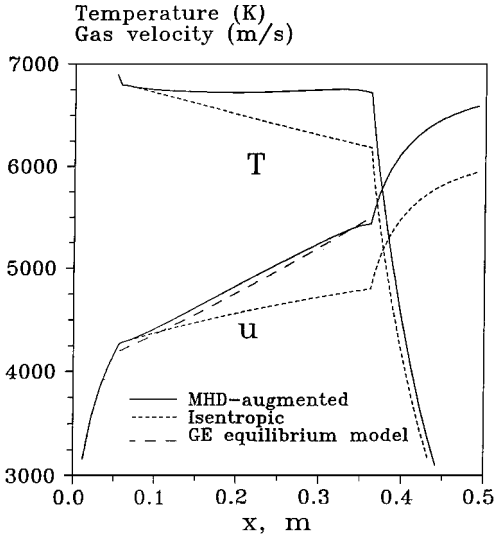

Fig. 1 Axial temperature and velocity profiles for the GE reflected shock unseeded air accelerator.

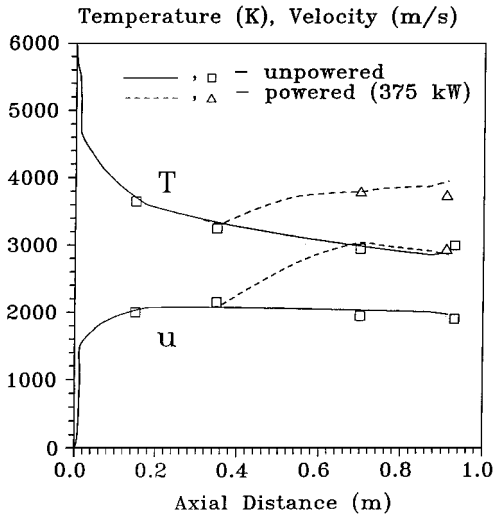

Fig. 2 Experimental and calculated temperature and velocity axial profiles for the AEDC potassium-seeded accelerator.

and so the electron temperature was very close to the gas temperature throughout the channel. The predicted electric conductivity is in good agreement with the measured value, $\sigma = 110$ mho/m. Calculations show that the flow quality in the test section is poor. The atom fractions remain frozen at the MHD channel temperature and reach 10% for N atoms and 30% for O atoms. The calculated flow power increase for these experiments is about 25%, from 20 to 25 MW, which corresponds to a total enthalpy increase from 24 to 30 MJ/kg.

The second series of calculations was made for the Arnold Engineering Development Center (AEDC) continuous-mode MHD accelerator running on potassium-seeded (at 1.5%) nitrogen (accelerator B of Ref. 37). In these experiments, nitrogen was heated by an arc up to $T_0 = 6000$ K at a pressure $P_0 = 3.3$ atm and expanded through a MHD channel ($L = 77$ cm, $F_1 = 4\,\text{cm}^2$, $F_2/F_1 = 2.1$, and $B = 1.5$ T). Figure 2 shows the temperature and the flow velocity profiles along the channel. One can see that experimental and calculated data are in good agreement, temperature and pressure in the MHD-augmented flow being up to 30–50% higher than in the isentropic flow. Nonequilibrium effects in the channel are both insignificant because the temperature $T < 4000$ K is too low to stimulate thermal dissociation of nitrogen, whereas fast N_2 V-T relaxation on K atoms and slow expansion prevented freezing of nitrogen vibrations. Again, the effective reduced electric field was low, $(E/N)_{\text{eff}} \cong 1$ Td, so that $T_e \cong T$ in the channel. The estimated boundary-layer thickness[36] $\delta(x)/h = 0.37 \cdot Re_x^{-0.2} \cdot (x/h)$ gives $\delta(x)/h \cong 1$ already at $x/L = 0.5$. Indeed, the experiments show that the boundary layers in the channel overlap,[37] which results in significant power loss. Experiments[37] and present calculations show that, in the fully powered accelerator (power loading of 375 kW), up to 30% of the initial flow power of 640 kW is lost in heat transfer to the walls. Both measured and calculated total enthalpy increases for the fully powered accelerator are about 25%, from 7.6 to 9.5 MJ/kg.

In both series of calculations, the agreement with the experiments is quite good. We note, however, that additional model validation is desirable, in particular for MHD flows where the flow is far from thermal and ionization equilibrium.

III. Results and Discussion

We applied the kinetic model described and validated in Sec. II to modeling of both alkali-seeded and unseeded airflows in MHD accelerators in a wide range of plenum conditions and for various nozzle geometries. All subsequent calculations are made for the nozzle throat cross-sectional area $F = 4\,\text{cm}^2$ and ideal Faraday accelerator [$E_x = \beta \cdot (E_y - uB_z)$, $j_x = 0$] with the magnetic field in the channel $B_z = 10$ T. The secondary expansion duct was assumed to be 2 m long with the exit area of 9 m^2.

A. Unseeded Flows

The first series of runs was made for dry air for the plenum temperatures $T_0 = 3000$–6000 K and plenum pressures $P_0 = 10$–1000 atm. The MHD channel parameters were $L = 30$ cm, $F_1 = 8\,\text{cm}^2$, and $F_2/F_1 = 2$ (geometry similar to the GE MHD channel[39,40]). In all cases, the channel entrance Mach number was $M = 2$, and the channel entrance pressure was about 10% of P_0. Constant loading parameter $K = E_y/uB_z = 2$ was assumed. Ionization in the channel was sustained by a relativistic e-beam. The constant e-beam loading per molecule was in the range $D = 0.0$–1.0 keV/mol/s.

Figure 3 summarizes the results obtained. It shows the total enthalpy of flow H as a function of entropy S for $D = 1.0$ keV/mol/s. The exceptions are runs 6 and 3 for which the beam load was taken to be $D = 0.3$ and 0.1 keV/mol/s, respectively, to avoid thermal instability. One can see that the total enthalpy increase is small unless the plenum pressure is low. Only for the plenum pressure of $P_0 = 10$ atm (channel pressure $\leq$ 1atm) does the nonequilibrium ionization provide a substantial flow power increase at reasonable efficiency ($\Delta H/H_0 = 0.5$–2.0 and $\Delta Q_{\text{beam}}/\Delta H = 0.03$–$0.05$). At higher plenum pressures the flow power increase does not exceed 10–20%

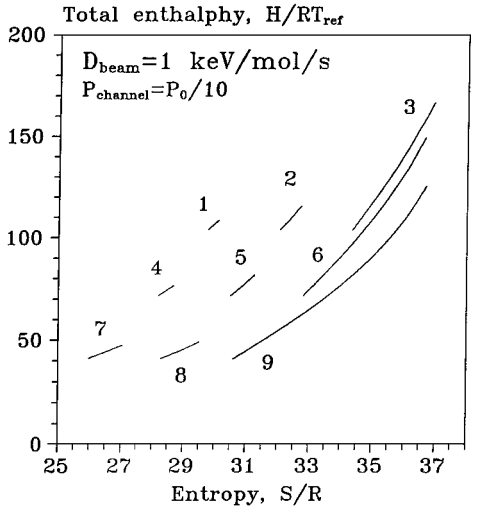

Fig. 3 Total enthalpy vs entropy for the MHD-augmented unseeded airflows, ionized by a high-energy e-beam: 1, $T_0 = 6000$ K and $P_0 = 1000$ atm; 2, $T_0 = 6000$ K and $P_0 = 100$ atm; 3, $T_0 = 6000$ K and $P_0 = 10$ atm; 4, $T_0 = 4500$ K and $P_0 = 1000$ atm; 5, $T_0 = 4500$ K and $P_0 = 100$ atm; 6, $T_0 = 4500$ K and $P_0 = 10$ atm; 7, $T_0 = 3000$ K and $P_0 = 1000$ atm; 8, $T_0 = 3000$ K and $P_0 = 100$ atm; 9, $T_0 = 3000$ K and $P_0 = 10$ atm.

($\Delta H/H_0 < 0.2$), and it is mainly due to gas heating in recombination processes ($\Delta Q_{\text{beam}}/\Delta H = 0.6$–$1.0$). Obviously, at the high number densities the electron loss rate is so fast that the ionization fraction n_e/N sustained by the beam becomes too low to produce a noticeable Lorentz force. For example, for $D = 0.3$ keV/mol/s, $n_e/N \sim 10^{-5}$ at the channel pressure of 1 atm, $n_e/N \sim 10^{-6}$ at 10 atm, and $n_e/N \sim 10^{-7}$ at 100 atm. Because the total power addition in the full-scale, high-pressure wind tunnel has to be $\Delta H \sim 1$ GW and at the high channel pressure conditions $\Delta Q_{\text{beam}}/\Delta H \sim 1$, this would require the use of a ~1-GW e-beam (in a very inefficient way). We emphasize that the low efficiency at high pressures is due to the high rate of electron loss, which is independent of the method of nonequilibrium ionization. Because the high-energy e-beam is the most efficient ionization source available (see Sec. II.B), the use of other methods of external ionization in the high-pressure MHD channels ($P > 1$ atm) is also not feasible.

Thus, the only way to efficiently use an external ionization source in high plenum pressure flows is to expand the flow down to the low pressures before creating nonequilibrium ionization. We considered the feasibility of this mode of operation in the second series of calculations for $T_0 = 3000$–6000 K, $P_0 = 1000$ atm, and $D = 1$ keV/mol/s. The MHD channel parameters were $L = 30$ cm, $F_1 = 170$ cm^2, $F_2/F_1 = 2.35$, and $K = 2 = \text{const}$. The channel entrance Mach number now was $M = 5$, and the channel pressure was about 1 atm. The results shown in Fig. 4 demonstrate a considerable total enthalpy rise (up to 70%) and reasonable beam efficiency ($\Delta Q_{\text{beam}}/\Delta H \sim 0.05$–$0.1$) for the high plenum and channel temperatures. Higher temperatures result in 1) a compensation of electron attachment by thermal detachment from the negative ions and 2) a slower recombination rate at the lower number density.

It is easy to see that on the Mollier charts (Figs. 3 and 4) the slope $\mathrm{d}H(S)/\mathrm{d}S$ is

$$\tan\varphi = \frac{\mathrm{d}H}{\mathrm{d}S} = \frac{\mathrm{d}Q_{\text{total}}}{\mathrm{d}Q_{\text{thermal}}}T = \frac{\boldsymbol{j}\cdot\boldsymbol{E}}{\boldsymbol{j}\cdot\boldsymbol{E} - \boldsymbol{u}\cdot(\boldsymbol{j}\times\boldsymbol{B})}T$$

$$= \frac{\sigma K(K-1)u^2B_z^2}{\sigma(K-1)^2u^2B_z^2}T = \frac{K}{K-1}T \qquad (3)$$

where $\mathrm{d}Q_{\text{total}}$ and $\mathrm{d}Q_{\text{thermal}}$ are the total power added to the flow and the power going into heating, respectively. Therefore, the flow entropy rise ΔS for the given total enthalpy increase ΔH is controlled by the average temperature at which the energy is added to the flow T_{avg} and by the loading parameter $K > 1$. MHD accelerators sustained by external ionization are less effective than the seeded accelerators because the flow expansion before the MHD channel needed to reduce the pressure also results in the low channel entrance temperature. For the cases shown in Fig. 4, $T_{\text{avg}} = 1300$, 2400, and 4400 K, the steepest slope $\mathrm{d}H/\mathrm{d}S$ corresponds to the highest value of T_{avg}. Reducing the loading parameter would not increase $\tan(\varphi)$ because it would also reduce the total power added to the flow $\mathrm{d}Q_{\text{total}} \sim K(K-1)$ [see Eq. (3)] and inhibit the Joule heating, which would result in further reduction of T_{avg}.

The third series of calculations for the full-scale accelerator was made for $T_0 = 5000$ K, $P_0 = 1000$ atm, $G = 17.4$ kg/s, and $D = 0.0$–2.0 keV/mol/s. The MHD channel parameters now were $L = 140$ cm, $F_1 = 200$ cm^2, and $F_2/F_1 = 1.65$ (entrance Mach number $M = 5$ and channel pressure $P = 1$–2 atm). To prevent the large-scale thermal instability (see Sec. III.C) leading to runaway gas heating in the channel, the loading parameter at high temperatures was reduced: $K = 1.5$ at $T < 2500$ K, $K = 1.0 + 0.5 \times (T/2500)$ at $T \geq 2500$ K.

The results of calculations are shown in Figs. 5–7. Figure 5 presents the obtained $H(S)$ curves, plotted together with the target values for a transatmospheric vehicle (TAV) trajectory. One can see that, although the total enthalpy of the flow increases 1.5–2.5 times, the flow entropy is greater than the target values. The reason for that, as discussed earlier, is the low MHD channel temperature [see Fig. 6 and Eq. (3)]. Therefore, although the Mach numbers in the MHD-augmented flow are close to the target values, the flow pressure is ~10–30 times lower than the pressure behind the bow shock (Table 1).

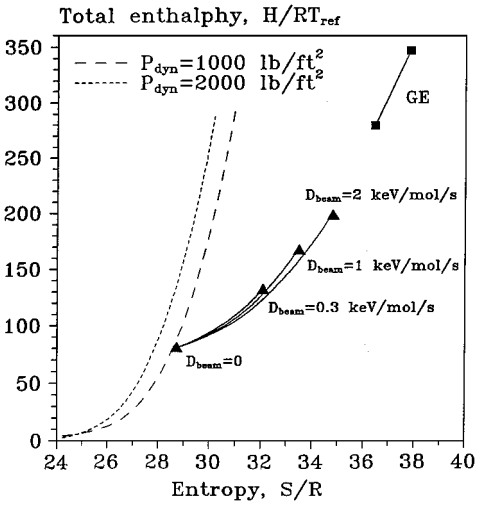

Fig. 5 Total enthalpy vs entropy for the full-scale unseeded air MHD accelerator with external ionization by an e-beam; $P_0 = 1000$ atm, $T_0 = 5000$ K, $L = 140$ cm, and $F_2/F_1 = 1.65$. Dashed lines indicate TAV trajectories. Also shown is $H(S)$ for the GE reflected shock unseeded air accelerator.

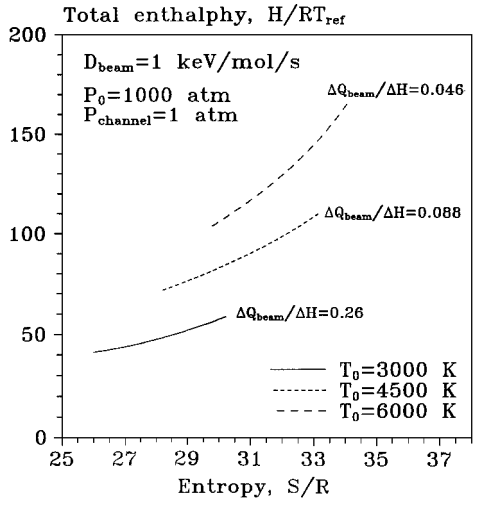

Fig. 4 Total enthalpy vs entropy for the high-plenum-pressure MHD-augmented unseeded airflows, ionized by a high-energy e-beam. The flow is expanded to $P \sim 1$ atm before entering the MHD channel.

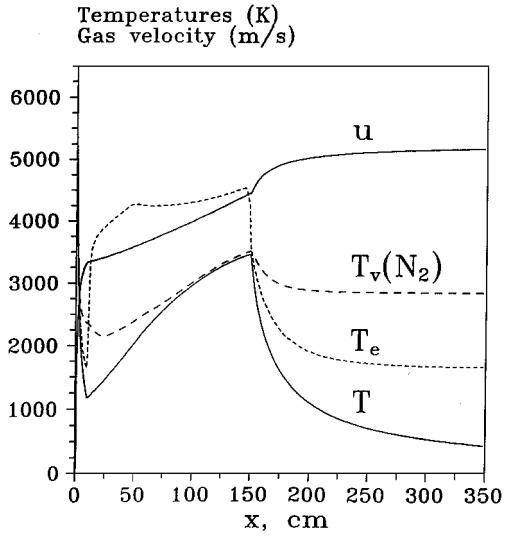

Fig. 6 Axial profiles of the translational temperature, vibrational temperature of nitrogen, and electron temperature for the accelerator of Fig. 5 for $D_{\text{beam}} = 1$ keV/mol/s.

Table 1 Unseeded air MHD accelerator performance; left and central subcolumns show target values for P_{dyn} = 2000 and 1000 lb/ft^2, respectively, and right subcolumn shows present calculations

Case no.	H, MJ/kg			S/R			u, km/s			M		
1	7.2	7.0	6.9	27.9	28.6	28.9	3.76	3.64	3.60	9.4	9.0	8.9
2	11.6	11.0	11.4	28.7	29.3	32.1	4.78	4.58	4.60	10.9	10.4	10.4
3	13.6	14.6	14.5	29.0	29.9	33.5	5.16	5.31	5.15	11.4	11.3	10.9
4	15.8	16.9	17.2	29.3	30.2	34.8	5.58	5.71	5.49	11.8	11.8	10.9

Case no.	P, mbar			O, %	NO, %	$T_v(N_2)$	D, keV/mol/s	ΔQ_{beam}, MW	ΔH, MW
1	41.1	21.4	12.8	0.4	7.0	1574	0.0	0.0	0
2	35.7	18.5	2.0	1.5	6.2	2776	0.3	6.5	77
3	34.4	17.2	1.3	5.6	6.2	2857	1.0	21	130
4	33.1	16.1	1.3	14.7	6.2	2455	2.0	41	176

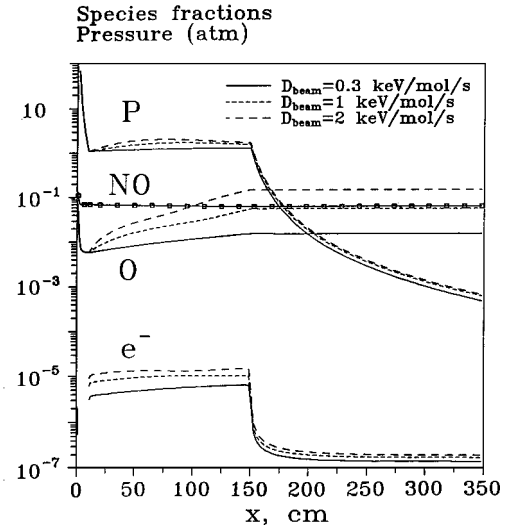

Fig. 7 Axial profiles of pressure and species mole fractions for the accelerator of Fig. 5 for different beam loads.

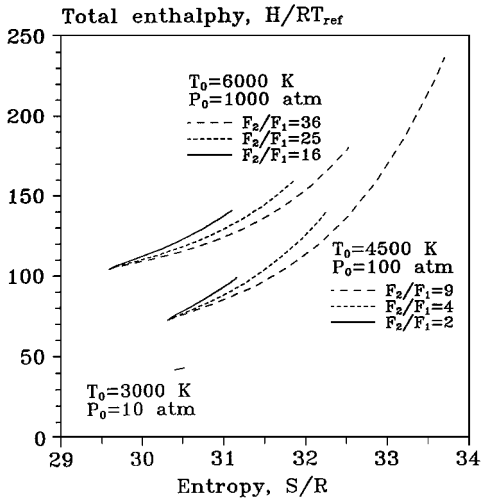

Fig. 8 Total enthalpy vs entropy diagram for the MHD-augmented K-seeded (at 1%) airflows.

Raising the beam load increases both recombination losses and the ratio $\Delta Q_{beam}/\Delta H$ (Table 1). This makes greater the average loading parameter K_{avg}, defined as the ratio of the total power into heating to the total power into kinetic energy. For this reason the slope dH/dS decreases with the beam load even though T_{avg} becomes higher (Fig. 5).

The calculated transverse current density in the channel did not exceed $j_y = 10$ A/cm^2. Both Joule heating and e-beam electrons induce flow dissociation in the channel, raising O atom fraction at the exit (Fig. 7). At the same time, the exit NO concentration changes very weakly (Fig. 7 and Table 1). This type of behavior simply reflects the dependence of equilibrium concentration of these species on temperature at $P \cong 1$ atm at the channel exit, which was verified by the equilibrium chemical composition data. Higher-than-equilibrium O and NO exit fractions at $D = 0$ (Table 1) are due to their large initial concentrations in the high-temperature plenum. Even though the flow becomes close to the vibrational equilibrium toward the end of the channel (Fig. 6), the flow in the test section is far from being at equilibrium (see Figs. 6 and 7 and Table 1). Both molecular vibrations and chemical composition are frozen in the rapid expansion occurring at low pressure and temperature. This effect can be reduced 1) if the energy is added at the high pressure (which in this case is not feasible), so that the relaxation in the secondary expansion becomes faster, or 2) if slower expansion is used.

Finally, Table 1 shows that one would need a tens-of-megawatts ionization source to operate the full-scale facility at the channel pressure of about 1 atm. The beam efficiency can be improved by further reducing the channel pressure, but this would lead to even greater flow entropy rise because of the lower channel entrance temperature [see Eq. (3)]. The electron beam load D can be simply related to the beam current density j_{beam} and the energy of the beam electrons ε_{beam} that determines the beam penetration length:

$$l \approx 0.5 \cdot \left(\frac{\varepsilon_{beam}}{300}\right)^{1.35} \cdot \frac{1.2}{\rho} \tag{4}$$

where l is in meters, ρ is in kilograms per cubic meter, and ε_{beam} is in kiloelectron volts.[19] For the conditions of Table 1, $l \cong 0.2$ m and $\Delta Q_{beam} = eDN\cdot(Ll^2) \cong j_{beam}\varepsilon_{beam}\cdot(Ll)$, one has $\varepsilon_{beam} \sim 30$ keV, and for $D = 1$ keV/mol/s, $j_{beam} \cong eDNl/\varepsilon_{beam} \cong 0.3$ A/cm^2.

B. Seeded Flows

The first series of runs was made for potassium-seeded (at 1%) air for the plenum temperatures $T_0 = 3000$–6000 K and pressures $P_0 = 10$–1000 atm. The MHD channel parameters were $L = 30$ cm, $F_1 = 8$ cm^2, and $F_2/F_1 = 2$–25. Again, in all calculated cases, the channel entrance Mach number was $M = 2$, and the entrance pressure was 10% of P_0. The results are shown in Fig. 8. All runs for $T_0 = 3000$ K did not show flow acceleration due to MHD augmentation because the electric conductivity was too low. Calculations for $T_0 = 4500$ K demonstrated noticeable total enthalpy rise ΔH only for the plenum pressures of $P_0 < 100$ atm. One can see from Fig. 8 that ΔH also increases with the channel area ratio, which results in the lower channel pressure. This is understandable because the flow acceleration is inversely proportional to the gas density:

$$\frac{du}{dt} \sim \frac{j_y B_z}{\rho} \sim \frac{\sigma(T) u B_z^2 (K-1)}{\rho} \tag{5}$$

where $\sigma(T)$ is proportional to the ionization fraction n_e/N. Thus, to produce the same acceleration at the higher pressure, a higher ionization fraction (and therefore a higher plenum temperature) is needed. Finally, substantial acceleration for $P_0 = 1000$ atm was obtained only at the highest plenum temperature considered, $T_0 = 6000$ K, also for the large area ratio $F_2/F_1 = 9$–25 (Fig. 8). One can see that the seeded MHD accelerator for the wind tunnel, which requires plenum pressures of a few thousand atmospheres, should operate at high plenum temperatures of $T_0 \sim 6000$ K and large MHD channel area ratios $F_2/F_1 \sim 25$.

The second series of runs was carried out for the full-scale cesium-seeded (at 0.5%) air accelerator for plenum conditions $T_0 = 5000$ K, $P_0 = 1000$ atm, and the mass flow rate $G = 17.4$ kg/s. The MHD

Table 2 Cs-seeded air MHD accelerator performance; left and central subcolumns show target values for P_{dyn} = 2000 and 1000 lb/ft^2, respectively, and right subcolumn shows present calculations

Case no.	H, MJ/kg			S/R			u, km/s			M		
1	7.2	7.0	6.7	27.9	28.6	28.3	3.76	3.64	3.53	9.4	9.0	9.1
2	13.6	14.6	14.1	29.0	29.9	30.8	5.16	5.31	5.14	11.4	11.3	11.5
3	18.4	19.4	19.7	29.6	30.4	31.4	6.02	6.14	6.07	12.3	12.2	12.3
4	24.8	25.7	25.2	30.2	31.0	31.9	6.99	7.07	6.88	13.1	13.0	13.1
5	33.2	33.8	33.9	30.9	31.6	32.5	8.08	8.12	7.98	13.9	13.8	13.7

Case no.	P, mbar			Cs, %	O, %	NO, %	$T_v(N_2)$	$j_{y\,max}$, A/cm^2
1	41.1	21.4	14.5	0.5	0.01	4.5	1992	0
2	34.4	17.2	3.9	0.5	0.6	4.3	2630	30
3	32.1	16.1	5.4	0.5	1.6	4.1	2829	50
4	30.4	15.3	6.3	0.5	2.9	4.2	2944	70
5	29.1	14.7	9.6	0.5	5.1	4.9	3078	100

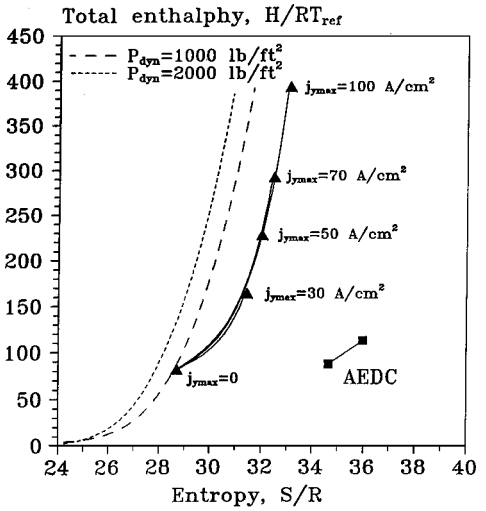

Fig. 9 Total enthalpy vs entropy for the full-scale Cs-seed (at 0.5%) air MHD; P_0 = 1000 atm, T_0 = 5000 K, L = 140 cm, and F_2/F_1 = 1.65. Dashed lines indicate TAV flight envelope. Also shown is $H(S)$ for the AEDC K-seeded (at 1.5%) accelerator.

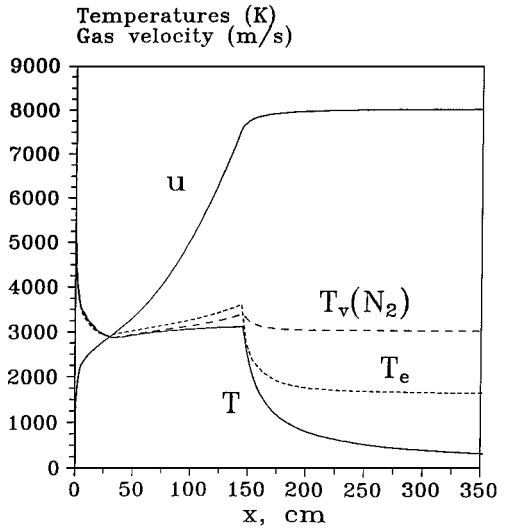

Fig. 10 Axial profiles of the translational temperature, vibrational temperature of nitrogen, and electron temperature for the accelerator of Fig. 10 for $j_{y\,max}$ = 100 A/cm^2.

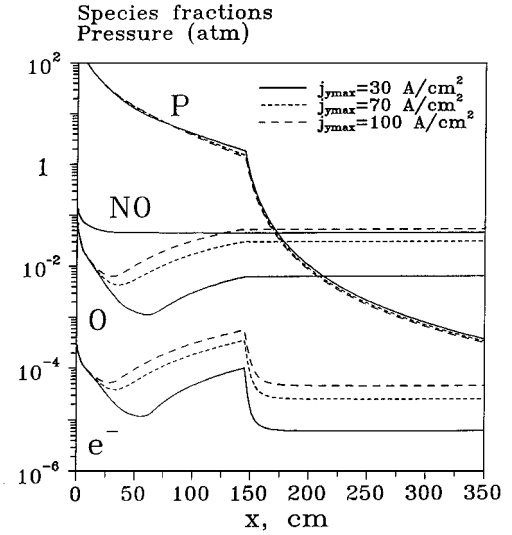

Fig. 11 Axial profiles of pressure and species mole fractions for the accelerator of Fig. 10 for different maximum current densities.

channel parameters were L = 140 cm, F_1 = 8 cm^2, and F_2/F_1 = 36 (channel entrance Mach number M = 2 and entrance pressure P = 120 atm). The loading parameter was again limited to prevent the development of the thermal instability (see Sec. III.C), $K = 1.0 + j_{ymax}/\sigma u B_z$. The calculated $H(S)$ curves are shown in Fig. 9 for different values of j_{ymax}, plotted together with the target TAV trajectory data. One can see that at these conditions the total enthalpy can be increased up to five times if the maximum current density does not exceed j_{ymax} = 100 A/cm^2, whereas the entropy rise is less than for the unseeded flows discussed in Sec. III.A (Fig. 5). Although the flow entropy is still greater than the target value, the seeded accelerator performance is clearly better. NO and O fractions in the test section are much smaller than in the unseeded accelerator at comparable total enthalpy (Tables 1 and 2). Also, the flow pressure is only 1.5–4.0 times less than the pressure behind the bow shock (Table 2).

The latter result is consistent with the criterion of Eq. (3). First, the average channel temperature in the seeded MHD accelerator is higher than in the e-beam-controlled channel (Figs. 6 and 10). Second, the average loading parameter in these runs is lower ($K_{avg} \cong$ 1.1–1.3 vs 1.6–1.8 for the unseeded runs), and so a greater part of the input power goes into the flow kinetic energy and does not contribute to the entropy rise. One can see from Fig. 10 that the efficiency of the first half of the channel is less than that of the second (du/dx is lower) due to the higher gas density near the channel entrance [see Eq. (5)]. The flow in the channel is close to the thermochemical equilibrium (Fig. 10), which is confirmed by the equilibrium chemical composition data. However, freezing of molecular vibrations (despite the fast V-T relaxation of N_2 on Cs and O atoms) and of chemical composition in the test section is still well pronounced (Figs. 10 and 11).

The boundary-layer thickness at the channel exit is $\delta/h \sim 0.25$. The calculated heat transfer losses did not exceed 15% of the initial flow power. However, the wall heat fluxes reach 10–20 kW/cm^2 for j_{ymax} = 100 A/cm^2, which may severely limit the operation time.

C. Flow Stability

The reduced electric field [see Eq. (2)] is quite low for all calculated regimes, $(E/N)_{eff} \leq 5$ Td for unseeded flows and $(E/N)_{eff} \leq 1$ Td for seeded flows. For this reason, the field-induced ionization

instability[35] in the core flow is unlikely. However, thermal instability due to the Joule heating might still develop. Using the stability analysis,[35] one obtains an expression for the large-scale instability increment in convectively cooled flows:

$$\Omega = \frac{K-1}{K}\frac{\gamma-1}{\gamma}\frac{j_y E_y}{P}\left(\frac{\delta \ell_n n_e}{\delta \ell_n T}+\frac{1}{2}\right)-\frac{2u}{L} \qquad (6)$$

Combining Eq. (6) with the expression for the quasi-steady-state electron density for the e-beam-sustained discharge or with the Saha equation, one obtains the instability threshold

$$j_y \le a\frac{K}{K-1}\frac{\gamma}{\gamma-1}\frac{P}{E_y}\frac{u}{L} \qquad (7)$$

In Eq. (7), $a = 8$ and $\frac{4}{3}$ for the recombination and attachment controlled discharges, respectively, and $a = (\frac{3}{8} + I/4T)^{-1}$ for equilibrium ionization. The recombination controlled discharge in air is realized only at high ionization fractions $n_e/N \ge 10^{-4}$, or high temperatures $T \ge 3000$ K, when thermal detachment from the negative ions compensates attachment. One can see that the equilibrium flow is less stable than the flow controlled by the external ionization: For $I/T \sim 10$–15, typical for the seeded MHD flows, one has $a \cong 0.2$–0.4. The criterion of Eq. (7), applied to the full-scale accelerators simulated in Secs. III.A ($K \cong 1.6$–1.8) and III.B ($K \cong 1.1$–1.3), predicts stable flow at $j_y \le 8$–10 and 40–100 A/cm^2, respectively. In both cases the channels operate on the verge of stability, which was the reason for the limiting of the loading parameter (see Secs. III.A and III.B). The same criterion, applied to experimental accelerators,[37,39] predicts stable core flow at $j_y \le 120$ A/cm^2 for the unseeded GE accelerator and at $j_y \le 15$ A/cm^2 for the K-seeded AEDC accelerator. In these experiments, where the stable core flow was indeed observed, the current densities did not exceed 20 and 15 A/cm^2, respectively.

This one-dimensional stability analysis cannot be applied to the boundary layer. It also does not allow analysis of the spoke instability.[41] The possibility of arcing in the boundary layer appears to be high for two reasons. First, the electric field in the sheath regions near the electrodes is higher than in the core flow,[35] which may result in a breakdown between the adjacent electrodes. Second, core flow Faraday mode conditions $E_x = \beta\cdot(E_y - uB_z)$, $j_x = 0$, assumed in the present calculations, will no longer hold in the boundary layer, which would result in the Hall current j_x flowing between the adjacent electrodes. This current can be very large because of the high recovery temperature and high scalar electric conductivity σ in the boundary layer. Both of these effects would short circuit the segmented electrodes along each wall, and the accelerator would run in a continuous electrode mode $E_x = 0$, $\sigma_{\text{eff}} = \sigma/(1+\beta^2)$ (Ref. 8). The effective electric conductivity σ_{eff} in the full-scale accelerator calculations, where $\beta_{\max} \sim 5$–10, would therefore be reduced by 1–2 orders of magnitude, making the accelerator performance much worse. These simple arguments are consistent with the observations made on the GE unseeded accelerator,[39] where the diffuse discharge in the core flow and arcing between each pair of electrodes on the same wall were observed.

Finally, the one-dimensional approach, where the electric and magnetic field profiles are assumed given (see Sec. II.A), does not allow determination of whether they can be operated at the stable conditions. A time-dependent, two-dimensional model, where the coupled flow equations, chemical kinetics equations, Maxwell equations, and Boltzmann equation are solved, is needed to address this problem, which is beyond the scope of the present paper.

D. Comparison with the Thermal Energy Addition Methods

If all of the energy added to the flow goes into heating, Eq. (3) simplifies:

$$\tan\varphi = \frac{\mathrm{d}H}{\mathrm{d}S} = T \qquad (8)$$

We estimate the average energy addition temperature for the pure heating, assuming that the flow conditions are the same as in case 2 of Table 2 ($\Delta H = 7.4$ MJ/kg, $\Delta S = 0.70$ kJ/kg/K, and post-bow-shock Mach number $M = 11.5$). These conditions correspond to the flight Mach number $M_{\text{flight}} \cong 18$. Equation (8) gives $T_{\text{avg}} \cong 10{,}000$ K, whereas the average temperature for the MHD energy addition is about 2500 K. This remarkable difference occurs because most of the power in the MHD channel goes directly into the flow kinetic energy ($K_{\text{avg}} \cong 1.34$ for case 2). Let us also estimate T_{avg} for pure heating from $T_0 = 2000$ K, $P_0 = 10{,}000$ atm, to the conditions of case 2, assuming that the caloric equation of state[28,29] is still valid at these pressures. One obtains $\Delta H = 12.1$ MJ/kg and $\Delta S = 2.67$ kJ/kg/K, giving $T_{\text{avg}} \cong 4500$ K (or $T_{\text{avg}} \cong 3800$ K for $T_0 = 1000$ K). This means that flow acceleration up to $M_{\text{flight}} \cong 18$ by means of thermal energy addition to the high-pressure airflow ($P_0 \sim 10^4$ atm) would require heating the gas to higher temperatures than obtained in the MHD accelerator. This would induce considerable chemical contamination of the flow.

IV. Conclusions

The results of the modeling calculations permit the following conclusions to be made.

1) The use of an electron beam (or any other external ionization source) to sustain nonequilibrium ionization in high-pressure MHD channels is not feasible due to the fast electron loss. In the high-plenum-pressure ($P_0 \sim 1000$ atm) flows, e-beams can be efficiently applied to create ionization only after the flow is expanded to the low pressures $P \le 1$ atm.

2) In the latter mode of operation, nonequilibrium ionization sustained by an e-beam allows increase in the total enthalpy of the flow (1.5–2.5 times, $M \sim 11$ in the test section) due to MHD augmentation. However, in this case the static pressures in the test section are 10–30 times lower than required by the TAV trajectory. Also, the flow quality is poor and gets steadily worse with the increase in the total enthalpy due to both e-beam-initiated dissociation and thermal chemical reactions.

3) The high-plenum-pressure ($P_0 \sim 1000$ atm), alkali-seeded flows, which also require high plenum temperatures ($T_0 \ge 5000$–6000 K), look more promising for the wind-tunnel application. Calculations for Cs-seeded flows predict an up-to-five-times total enthalpy increase (test section Mach number $M \sim 14$). Predicted test section static pressures are also closer to the target values (although they are still 1.5–4 times lower). The calculated oxygen atom and NO concentrations are also lower than for the unseeded flows.

4) The predicted test section flow parameters can be obtained in a flow stable with respect to large-scale thermal instability.

5) Simple thermodynamic analysis shows the advantage of adding energy to the flow by means of a body force over the purely thermal energy addition.

A two-dimensional, time-dependent kinetic model incorporating Maxwell equations is necessary to study the sheath and boundary-layer effects, as well as small-scale flow instabilities.

Acknowledgments

This research was sponsored by NASA as part of the MARIAH program and was conducted by the U.S. Department of Energy under a work-for-others agreement, DOE Contract DE-AC22-88ID12735. We would like to express our gratitude to Sergey Macheret from Princeton University for many useful discussions.

References

[1] Simmons, G., Nelson, G. L., Hiers, R., and Western, A., "An Unseeded Air MHD Accelerator Concept for High Mach Number Hypersonic Propulsion," AIAA Paper 89-2535, July 1989.

[2] Miles, R. B., Brown, G. L., Lempert, W. R., Yetter, R., Williams, G. J., Jr., and Bogdonoff, S. M., "Radiatively Driven Hypersonic Wind Tunnel," *AIAA Journal*, Vol. 33, No. 8, 1995, pp. 1463–1470.

[3] Nelson, G. L., and Simmons, G., "Augmentation of Hypersonic Propulsion Facilities Using MHD," AIAA Paper 95-1937, June 1995.

[4] Crawford, R. A., Chapman, J. N., and Rhodes, R. P., "Performance Potential and Technology Issues of MHD Augmented Hypersonic Simulation Facilities," AIAA Paper 90-1380, June 1990.

[5] Simmons, G. A., Nelson, G. L., and Lee, Y. M., "Analysis of an Unseeded, Nonequilibrium MHD Accelerator Concept for Hypersonic Propulsion Ground Testing Applications," AIAA Paper 92-3994, July 1992.

[6] Lineberry, J., and Chapman, J., "MHD Accelerators for Hypersonic Applications," AIAA Paper 91-0384, Jan. 1991.

[7] Clark, J. F., and McChesney, M., *Dynamics of Real Gases*, Butterworths, London, 1976, Chap. 2.

[8]Sutton, G. W., and Sherman, A., *Engineering Magnetohydrodynamics*, McGraw–Hill, New York, 1965, Chap. 3.

[9]Adamovich, I. V., Macheret, S. O., Rich, J. W., and Treanor, C. E., "Vibrational Relaxation and Dissociation Behind Shock Waves Part 2: Master Equation Modeling," *AIAA Journal*, Vol. 33, No. 6, 1995, pp. 1070–1075.

[10]Gordiets, B. F., and Zhdanok, S., "Analytical Theory of Vibrational Kinetics of Anharmonic Oscillators," *Nonequilibrium Vibrational Kinetics*, edited by M. Capitelli, Springer, Berlin, 1986, pp. 47–83.

[11]Huxley, L. G. H., and Crompton, R. W., *The Diffusion and Drift of Electrons in Gases*, Wiley, New York, 1974, Chaps. 6 and 8.

[12]Dyatko, N. A., Kochetov, I. V., and Napartovich, A. P., "Electron Energy Distribution Function in Decaying Nitrogen Plasmas," *Journal of Physics D: Applied Physics*, Vol. 26, No. 3, 1993, pp. 418–423.

[13]Aleksandrov, N. L., Konchakov, A. M., and Son, E. E., "Electron Distribution Function and Kinetic Coefficients of a Nitrogen Plasma. II. Vibrationally Excited Molecules," *Plasma Physics Reports*, Vol. 4, No. 3, 1978, pp. 663–666.

[14]Aleksandrov, N. L., Konchakov, A. M., and Son, E. E., "Electron Distribution Function and Kinetic Coefficients of a CO Plasma. II. Vibrationally Excited Molecules," *Soviet Physics: Technical Physics*, Vol. 49, No. 12, 1979, pp. 1200–1204.

[15]Krivonosova, O. E., Losev, S. A., Nalivaiko, V. P., Mukoseev, Y. K., and Shatalov, O. P., "Recommended Data on Rates of Chemical Reactions Between Molecules Consisting of N and O Atoms," *Khimiya Plazmy (Plasma Chemistry)*, edited by B. M. Smirnov, Vol. 14, Nauka, Moscow, 1987, pp. 3–31.

[16]Macheret, S. O., Fridman, A. A., and El'kin, A. A., "Rates Constants of Exchange Reactions in Nonequilibrium Conditions: Classical Model," *Khimicheskaya Fizika (Soviet Chemical Physics)*, Vol. 9, No. 2, 1990, pp. 174–179.

[17]Macheret, S. O., and Rich, J. W., "Nonequilibrium Dissociation Rates Behind Strong Shock Waves," *Chemical Physics*, Vol. 174, No. 1, 1993, pp. 25–43.

[18]Treanor, C. E., Adamovich, I. V., Williams, M. J., and Rich, J. W., "Kinetics of NO Formation Behind Strong Shock Waves," *Journal of Thermophysics and Heat Transfer*, Vol. 10, No. 2, 1996, pp. 193–199.

[19]Matzing, H., "Chemical Kinetics of Flue Gas Cleaning by Irradiation with Electrons," *Advances in Chemical Physics*, edited by I. Prigogine and S. A. Rice, Vol. 80, Wiley, New York, 1991, pp. 315–403.

[20]Cool, T. A., and Zukoski, E. E., "Recombination, Ionization, and Nonequilibrium Electrical Conductivity in Seeded Plasmas," *Physics of Fluids*, Vol. 9, No. 4, 1966, pp. 780–796.

[21]Ashton, A. F., and Hayhurst, A. N., "Kinetics of Collisional Ionization of Alkali Metal Atoms and Recombination of Electrons with Alkali Metal Ions in Flames," *Combustion and Flame*, Vol. 21, No. 1, 1973, pp. 69–75.

[22]Olson, R. E., "Absorbing-Sphere Model for Calculating Ion-Ion Recombination Total Cross-Sections," *Journal of Chemical Physics*, Vol. 56, No. 6, 1972, pp. 2979–2984.

[23]Torr, D. G., "The Photochemistry of Upper Atmosphere," *The Photochemistry of Atmospheres*, edited by J. S. Levine, Academic, New York, 1985, pp. 165–280.

[24]Itikawa, Y., Hayashi, M., Ichimura, A., Onda, K., Sakimoto, K., Takayanagi, K., Nakamura, M., Nishimura, H., and Takayanagi, T., "Cross-Sections for Collisions of Electrons and Photons with Nitrogen Molecules," *Journal of Physical and Chemical Reference Data*, Vol. 16, No. 3, 1986, pp. 985–1010.

[25]Itikawa, Y., Ichimura, A., Onda, K., Sakimoto, K., Takayanagi, K., Hatano, Y., Hayashi, M., Nishimura, H., and Tsurubichi, S., "Cross-Sections for Collisions of Electrons and Photons with Oxygen Molecules," *Journal of Physical and Chemical Reference Data*, Vol. 18, No. 1, 1989, pp. 23–42.

[26]Mojarrabi, B., Gulley, R. J., Middleton, A. G., Cartwright, D. C., Teubner, P. J. O., Buckman, S. J., and Bringer, M. J., "Electron Collisions with NO: Elastic Scattering and Robivrational ($0 \rightarrow 1$, 2, 3, 4) Excitation Cross-Sections," *Journal of Physics B: Atomic, Molecular, and Optical Physics*, Vol. 28, No. 3, 1995, pp. 487–504.

[27]Lennon, M. A., Bell, K. L., Gilbody, H. B., Hughes, J. G., Kingston, A. E., Murray, M. J., and Smith, F. J., "Recommended Data on the Electron Impact Ionization of Atoms and Ions: Fluorine to Nickel," *Journal of Physical and Chemical Reference Data*, Vol. 17, No. 3, 1988, pp. 1285–1363.

[28]Glushko, V. P. (ed.), *Thermodynamic Properties of Individual Substances*, Nauka, Moscow, 1976, pp. 115–527.

[29]Chase, M. W., Davies, C. A., Downey, J. R., Frurip, D. J., McDonald, R. A., and Syverud, A. N., "JANAF Thermochemical Tables," *Journal of Physical and Chemical Reference Data*, Vol. 14, Supplement 1, Pt. 2, 1985, pp. 943–1695.

[30]Chen, J. C. Y., "Theory of Subexcitation Electron Scattering by Molecules. II. Excitation and De-Excitation of Molecular Vibrations," *Journal of Chemical Physics*, Vol. 40, No. 12, 1964, pp. 3513–3520.

[31]Adamovich, I. V., Macheret, S. O., Rich, J. W., and Treanor, C. E., "Nonperturbative Analytic Theory of V-T and V-V-T Rates in Diatomic Gases, Including Multi-Quantum Transitions," AIAA Paper 95-2060, June 1995.

[32]Fisher, E. R., and Smith, G. K., "Alkali Quenching in High Temperature Environments," *Chemical Physics Letters*, Vol. 13, No. 5, 1972, pp. 448–452.

[33]Eremin, A. V., Kulikovsky, A. A., and Naboko, I. M., "Sodium Excitation in Non-Equilibrium Conditions Behind Shock Waves in Nitrogen," *Chemical Physics Letters*, Vol. 45, No. 2, 1976, pp. 351–355.

[34]Perel, J., Englander, P., and Bederson, B., "Measurement of Total Cross-Sections for the Scattering of Low-Energy Electrons by Lithium, Sodium, and Potassium," *Physical Review*, Vol. 128, No. 3, 1962, pp. 1148–1154.

[35]Raizer, Y. P., *Gas Discharge Physics*, Springer, Berlin, 1991, Chap. 14.

[36]Schlichting, H., *Boundary Layer Theory*, McGraw–Hill, New York, 1960, Chap. 21.

[37]Rittenhouse, L. E., Pigott, J. C., Whoric, J. M., and Wilson, D. R., "Theoretical and Experimental Results with a Linear Magnetohydrodynamic Accelerator Operated in the Hall Current Neutralized Mode," Arnold Engineering Development Center, AEDC-TR-67-150, Tullahoma, TN, Nov. 1967.

[38]Gallagher, J. W., Beaty, E. C., Dutton, J., and Pitchford, L. C., "An Annotated Compilation and Appraisal of Electron Swarm Data in Electronegative Gases," *Journal of Physical and Chemical Reference Data*, Vol. 12, No. 1, 1983, pp. 109–152.

[39]Warren, W. R., Harris, C. J., and Marston, C. H., "Feasibility Study of a High Density Shock Tunnel Augmented by a Magneto-Hydrodynamic Accelerator," Arnold Engineering Development Center, AEDC-TR-65-225, Arnold Air Force Station, TN, Oct. 1965.

[40]Harris, C. J., Marston, C. H., and Warren, W. R., "MHD Augmented Shock Tunnel Experiments with Unseeded, High Density Air Flows," *AIAA Journal*, Vol. 13, No. 1, 1975, pp. 229–231.

[41]Rosa, R. J., *Magnetohydrodynamic Energy Conversion*, McGraw–Hill, New York, 1968, Chap. 3.

W. Oberkampf
Associate Editor